Cerebral Cortex January 2013;23:178–186
doi:10.1093/cercor/bhr393
Advance Access publication January 23, 2012

Human Parietofrontal Networks Related to Action Observation Detected at Rest

Elisa Molinari[1], Patrizia Baraldi[2], Martina Campanella[1], Davide Duzzi[2], Luca Nocetti[3], Giuseppe Pagnoni[2] and Carlo A. Porro[2]

[1]Department of Robotics, Brain and Cognitive Sciences, Istituto Italiano di Tecnologia, 16163 Genova, Italy, [2]Dipartimento di Scienze Biomediche, Universita' di Modena e Reggio Emilia, 41125 Modena, Italy and [3]Servizio di Fisica Sanitaria, Azienda Universitaria-Ospedaliera Policlinico, 41125 Modena, Italy

Address correspondence to Patrizia Baraldi, Dipartimento di Scienze Biomediche, Via Campi 287, I-41125 Modena, Italy. Email: patrizia.baraldi@unimore.it.

Recent data show a broad correspondence between human resting-state and task-related brain networks. We performed a functional magnetic resonance imaging (fMRI) study to compare, in the same subjects, the spatial independent component analysis (ICA) maps obtained at rest and during the observation of either reaching/grasping hand actions or matching static pictures. Two parietofrontal networks were identified by ICA from action observation task data. One network, specific to reaching/grasping observation, included portions of the anterior intraparietal cortex and of the dorsal and ventral lateral premotor cortices. A second network included more posterior portions of the parietal lobe, the dorsomedial frontal cortex, and more anterior and ventral parts, respectively, of the dorsal and ventral premotor cortices, extending toward Broca's area; this network was more generally related to the observation of hand action and static pictures. A good spatial correspondence was found between the 2 observation-related ICA maps and 2 ICA maps identified from resting-state data. The anatomical connectivity among the identified clusters was tested in the same volunteers, using persistent angular structure–MRI and deterministic tractography. These findings extend available knowledge of human parietofrontal circuits and further support the hypothesis of a persistent coherence within functionally relevant networks during rest.

Keywords: anatomical connectivity, functional connectivity, functional magnetic resonance imaging, independent component analysis, tractography

Introduction

Brain function is thought to be critically dependent on the integrated activity of neuronal assemblies, over different temporal and spatial scales (Ioannides 2007; Tononi 2010). The dynamics and interactions among large-scale neural systems can be indirectly investigated using noninvasive functional imaging techniques, such as blood oxygenation level–dependent (BOLD) functional magnetic resonance imaging (fMRI). Even in the absence of specific tasks, namely during the so-called resting-state condition, arrays of cortical regions showing coherent BOLD-fMRI fluctuations can be consistently detected across human subjects (Damoiseaux et al. 2006), possibly reflecting the organization of a series of highly coherent neuronal networks (Sadaghiani et al. 2010; Deco et al. 2011).

A recent study (Smith et al. 2009) has shown that many of the major functional networks in the human brain, identified by independent component analysis (ICA) from thousands of tests of explicit brain activation conditions in fMRI and positron emission tomography (PET) studies, are spatially similar to resting-state brain networks, as identified by fMRI and ICA in healthy volunteers. The results by Smith and colleagues lend therefore strong support to the hypothesis of an ongoing interconnection of functionally relevant brain circuits, even in the resting-state. However, their data deal primarily with a relatively small number of broadly defined functional networks (e.g., sensorimotor, cognitive/language, etc.). More direct evidence for a spatial correspondence between rest and task-related networks could derive from the comparison of brain activity in the same volunteers, using experimental paradigms suitable to investigate more specific functions.

In the present study, we compared parietofrontal networks identified at rest and in 2 activation tasks, during which subjects were viewing either video clips of a hand grasping an object (action observation) or single frames showing a still hand and object (static-scene observation). Action observation–related activity has been extensively investigated in the human brain (for a recent meta-analysis, see Caspers et al. 2010) and represents therefore a relevant framework for testing the above-mentioned hypothesis. Indeed, specific parietofrontal circuits are considered to be the core of the human mirror system, which is likely to be involved in several cognitive and motor functions (Rizzolatti and Craighero 2004; Catmur et al. 2009; Gallese 2009). The anatomical connections of parietofrontal circuits have been mapped in the monkey (e.g., Rozzi et al. 2006; Borra et al. 2008) and are beginning to be understood in humans (Tomassini et al. 2007; Frey et al. 2008); however, there is relatively little information as to how the nodes of this system are functionally connected in the human brain, especially when no specific visual stimuli are presented.

To address this issue, we performed an fMRI study and compared spatial ICA maps of the left hemisphere obtained at rest and during the observation tasks in the same group of healthy volunteers. The anatomical connectivity between selected clusters of the ICA maps was then tested using persistent angular structure (PAS)–MRI (Jansons and Alexander 2003; Jiang et al. 2007) and deterministic tractography.

Materials and Methods

We studied 16 healthy volunteers (9 females and 7 males; mean age 23.3 ± 6.7 years) after informed consent and approval of the Committee on Ethics of the University of Modena and Reggio Emilia. All volunteers were right handed, as assessed using the Edinburgh Inventory (Oldfield 1971), and had normal or corrected-to-normal vision. Volunteers received a small monetary compensation for taking part in the experiment.

Tasks

All volunteers underwent one resting-state fMRI acquisition session (REST), lasting 306.6 s, during which they were instructed to relax with their eyes open while viewing a gray screen.

After the rest scan, 14 of them also performed 2 observation tasks, in an event-related paradigm. In one task, they looked at video sequences showing a right hand action, namely reaching for and precision grip of a small graspable object (MOVE stimuli; see example in Fig. 1). The

Figure 1. Representative frames from a video clip presented during the observation task.

object list included: a tape roll, a small battery, a little ball, clothes pegs, coins, an Italian-type coffee-maker, a coffee cup, a mug, a plug, a rubber, a rubber stamp, a knob, and a small knob. If relatively large objects (e.g., the coffee-maker) were the target of hand actions, grasping was directed to their handles; therefore, hand and finger movements were similar in all videos. During the other task, volunteers looked at static images showing a right hand and an object (STAT stimuli; see example in Fig. 1, leftmost picture). Each object was presented only once during either observation task. We chose to present videos showing movements of the hand and forearm (acting hand) rather than a full view of a person grasping an object (acting person) in order to reduce the complexity of the visual scene and thus focus volunteers' attention on the intended movement. Volunteers were instructed to look carefully at the pictures and to refrain from moving any part of their body throughout the experiment. Video clips were presented using the IFIS-SA H/W system (MRI Devices Corp., Waukesha, WI), and custom-made software was employed to control their delivery (http://digilander.libero.it/marco_serafini/stimoli_video/).

For each kind of observation task (MOVE or STAT), 2 runs lasting 306.6 s (7 events per run) were performed. At the beginning of each run, a uniform gray screen (baseline) was presented for 21 s. Each event consisted of a 4.2 s presentation of either a MOVE or an STAT stimulus, preceded by a visual alerting cue (the screen turning red for 2.1 s). The gray baseline screen was presented during the interstimulus intervals, with a variable duration within and between runs (mean = 40.36 s; range 35–46.9 s).

fMRI Data Acquisition

BOLD-sensitive fMRI images were acquired on a 3-T 16-channel Achieva scanner (Philips Medical Systems, Best, the Netherlands), using a gradient-echo echo-planar T_2^*-weighted sequence (time repetition [TR] = 700 ms; time echo [TE] = 35 ms; flip angle [FA] = 70°; field of view [FOV] = 220 mm; 438 volumes), from 12 oblique slices (no gap between slices; interleaved acquisition; 3.75 × 3.75 × 3.75 mm voxels) covering the parietal and frontal cortices of the left hemisphere and the adjacent right medial cortex (see Supplementary Fig. 1S). The short TR value was chosen as a trade-off between increasing the sampling of the hemodynamic response and obtaining a sufficient brain coverage; the left hemisphere was selected because of previous studies showing that it is preferentially involved during the observation of right hand actions (see Ortigue et al. 2010).

A whole-head high-resolution T_1-weighted image (3D-FFE sequence; TR = 35 ms, TE = 5.7 ms, FA = 50°, voxel size: 0.479 × 0.479 × 0.50 mm; 360 slices; sagittal orientation) was also acquired, for anatomical reference.

fMRI Data Analysis

Functional data analysis was carried out using the software packages AFNI (Cox 1996) (http://afni.nimh.nih.gov/afni), FSL (Smith et al. 2004) (http://www.fmrib.ox.ac.uk/fsl), and SPM5 (Friston et al. 2006) (http://www.fil.ion.ucl.ac.uk/spm/).

Observation tasks data and "resting-state" data were analyzed within the probabilistic ICA (pICA) framework (Beckmann and Smith 2004). To facilitate comparison with the existing literature, observation tasks data were also analyzed using the classical general linear model (GLM) (Friston et al. 1995): see Supplementary Material.

Probabilistic Independent Component Analysis

The only preprocessing step consisted in motion correction and was performed on all functional volumes using the FSL MCFLIRT routine.

Resting-state run. Resting-state functional connectivity (RSFC) was assessed by performing pICA on the fMRI time series, using the software tool "'Melodic"' (3.09) from the FSL package.

In order to identify groupwise regularities in the functional connectivity patterns, a 2-tier ICA procedure was employed (Pagnoni et al. 2006). A first-level pICA analysis, with automatic estimation of the number of components as implemented in Melodic (Beckmann and Smith 2004), was initially performed for each individual subject's data in the original acquisition space, yielding an ensemble of statistically independent spatial modes of functional connectivity (ICA *Z*-score brain maps), and their associated time courses. The individual ICA *Z*-score maps and the anatomical oblique data sets were then resliced along the standard cardinal axes. For each subject, the anatomical volume was coregistered to the average of the functional volumes and warped to standard Montreal Neurological Institute (MNI) template using the SPM5 tissue segmentation routines (Ashburner and Friston 2005); the individual ICA *Z*-score maps were then also spatially normalized by applying the set of warping parameters obtained from the MNI transformation of the anatomical volume.

All the individual warped and unthresholded *Z*-score maps were concatenated to form a composite group data set, similar to a volume time series but with the "time" dimension now indexing different ICA components and subjects; a second pICA procedure was then performed on the composite data set to yield group spatial modes. The number of components for the second-level ICA was arbitrarily set to 30, since 20–30 seems to be the most commonly chosen dimensionality according to previous studies (Damoiseaux et al. 2006; Smith et al. 2009; Zuo et al. 2010; Doucet et al. 2011), and it has been shown to be able to identify large- and medium-scale functional networks (Abou-Elseoud et al. 2010).

In order to assess the statistical significance of the group ICA maps, the contributions of individual subjects to the group maps were computed using the back-projection method (Calhoun et al. 2001), that is, as linear combinations of the subject's first-level ICA maps with the coefficients given by the subject-specific portion of the mixing matrix from the second-level ICA. ICA group maps represent a particular linear combination of all the input images, in our case, the first-level ICA maps from all subjects, according to coefficients represented by the mixing matrix. If we denote with S_j the jth group ICA spatial mode, we can split the associated column j of the mixing matrix, M_j, into contiguous sections corresponding to the input images from different subjects, $M_j = [M_{j,1}, M_{j,2}, \ldots, M_{j,n}]$, where n is the number of subjects. The linear combination of the input images belonging to a given subject k, $s_k = \{s_{k,1}, s_{k,2}, \ldots, s_{k,m}\}$ (where m is the estimated first-level ICA dimensionality for subject k), with the coefficients from the corresponding portion of the mixing matrix, that is, $M_{j,k} * s_k$, can then be taken as that subject's contribution to the group ICA map S_j.

The same back-projection procedure was also employed for reconstructing the individual time courses and power spectra associated with each group ICA mode. All components were evaluated by visual inspection of maps, time courses, and spectra, in order to exclude components related to artifacts. The individual contributions to the group spatial modes were finally entered into a 1-sample *t*-test across subjects (n = 16) to give a group *t*-statistic map for each second-level ICA spatial mode. Maps were thresholded at a combination of voxelwise $P < 0.01$ and cluster size > 10, to yield an experimentwise significance level of $P < 0.005$, corrected for multiple comparison (Forman et al. 1995), as determined by the AFNI routine AlphaSim. The specific combination of single-voxel P and cluster size threshold, among all the possible ones yielding a conservative level of experimentwise significance, was chosen in order to screen out very small

clusters and focus on medium-large-scale networks, which were the target of the present study.

Observation runs. The same 2-tier pICA approach described for the resting-state run was employed to detect task-related components from each task run, resulting in 2 sets of ICA components from the MOVE condition and 2 sets of ICA components from the STAT condition. As a result, we were also able to test reliability between runs corresponding to the same experimental condition.

Maps Correspondence and Identification of Task-Related Group ICA Components

The spatial similarity of maps related to different conditions was assessed by computing their spatial correlation coefficient r_s.

The identification of the task-related group ICA components from the observation runs was guided heuristically by the following criteria. First, we selected ICA components with a correlation coefficient r_t > 0.60 between their time course and the task profile (convolved with a canonical hemodynamic response function). Second, we considered these ICA components to be reliable only if they could be similarly identified in the 2 same task runs (either related to action or static-scene observation); more precisely, if the spatial correlation coefficient r_s between the selected ICA maps from the 2 runs exceeded 0.5.

Resting-state ICA maps similar to the identified task ICA maps were then selected; namely, for each task-related map, we chose the resting-state ICA map showing the highest r_s, with a screening threshold of 0.5.

The spatial overlap (SO) between maps was also computed as the percentage of voxels they had in common, relative to one map taken as reference.

Intersubject Variability

In order to evaluate the intersubject variability, we examined the action observation–related and the resting-state ICA components obtained from each subject's first-level pICA analysis. We adopted similar but less stringent criteria than those used in the ICA group analysis: namely, we selected ICA components from the action observation runs whose time course showed a correlation coefficient r_t > 0.40 with the task profile and resting-state ICA components showing an r_s > 0.3 with the chosen task-related ICA components. The spatial correspondence between the selected individual subjects' components and the action observation–related group ICA components was also evaluated.

Diffusion-Weighted Imaging Tractography

During the same scanning session, diffusion-weighted brain MRI (DWI) data were also obtained in all volunteers using a Spin Echo-Echo Planar Imaging sequence (FOV: 240 × 240 × 120 mm; voxel size: 1.875 × 1.875 × 2.1 mm; 57 slices; phase direction AP). A high angular resolution diffusion imaging (HARDI) approach (Tuch et al. 1999) with 64 isotropically distributed diffusion directions was used, with a b value of 1000 s/mm^2. Each b0 (unweighted) image was the average of 7 volumes. To test for repeatability, 2 DWI data sets were acquired in 14 out of 16 subjects.

Eddy current-induced image distortions were removed and brain masks obtained from the b0 images using the FSL software package (Smith 2002). The analysis and reconstruction of the diffusion-weighted data were carried out with the software package Camino (Cook et al. 2006).

In order to identify multiple fiber populations, PAS-MRI (Jansons and Alexander 2003) was performed to obtain the fiber orientation distribution (FOD). To speed up computation time, while maintaining good performance, a reduced encoding approach was adopted (Sweet and Alexander 2010), using only 16 of the encoding directions. The estimated fiber orientations were determined by the local maximum of FOD, setting 3 as the maximum number of peak directions in each voxel. A streamline tractography was then performed using a deterministic approach. Streamlines were generated from each point within the brain mask ("seeds"), using any of the following rules as stopping criteria: 1) an anisotropy value less than 0.2; 2) a curvature of the streamline of more than 80° across the voxel; and 3) entrance of the streamline into an out-of-brain voxel. A brain ventricles mask was created from the b0 image segmentation with a semiautomated method (Yushkevich et al. 2006) and applied to the tractography analysis as an exclusion mask in order to avoid unreliable tracts close to ventricles.

In order to investigate the degree of anatomical connectivity within resting-state circuits of interest, we identified tracts connecting pairs of clusters of the group parietofrontal ICA components obtained from the REST run. To this end, streamlines with opposing end points falling outside the extension of the chosen cluster pairs were discarded.

Results

fMRI Data—Group ICA Analyses

Several nonartifactual ICA maps could be identified from each action observation and static-scene observation run as well as from the resting-state run. Only maps including both parietal and frontal clusters are described here.

Two distinct parietofrontal ICA components (indicated hereafter as Network 1 and Network 2), whose time profiles had a correlation coefficient r_t >0.7 with the task profile, were identified from the action observation data (Fig. 2). A first IC (Network 1), found in both action observation runs (MOVE run1-IC4 and MOVE run2-IC3), showed a good spatial correspondence with a resting-state IC (REST-IC4) (see Fig. 3 and Table 1). A second IC (Network 2), identified as well in both action observation runs (MOVE run1-IC5 and MOVE run2-IC2), looked very similar to another resting-state IC (REST-IC1); notably, this component was also similar to an IC component identified from the 2 static-scene observation runs (STAT run1-IC1 and STAT run2-IC1) (Fig. 4 and Table 1).

The 2 networks identified in the action observation runs showed only minor spatial similarities, as indicated by their low spatial correlation coefficient and low SO (MOVE run1-IC4 and MOVE run2-IC2; r_s = 0.135; SO = 8.3%), as did the 2 corresponding components identified from the REST run (REST-IC4 and REST-IC1: r_s = 0.211; SO = 12.6%).

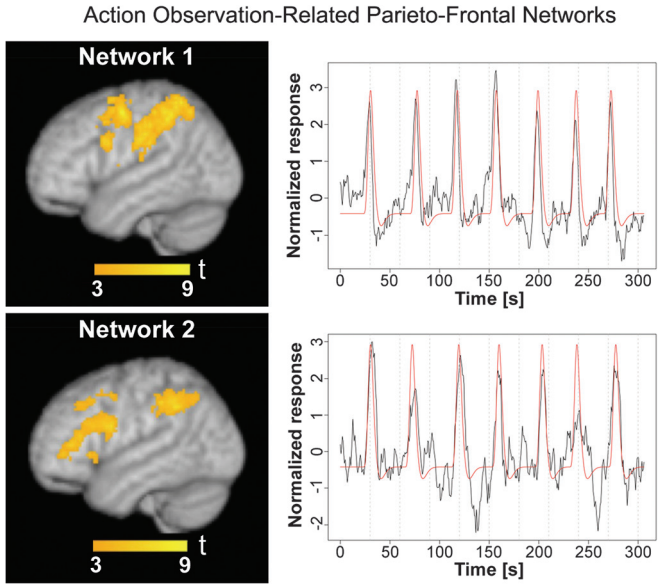

Figure 2. Two action observation–related nonoverlapping parietofrontal networks were identified by ICA from the MOVE runs. For each one, the best representative from the 2 runs, that is, the IC component with the highest correlation coefficient (r_t) between its time course and the task profile, is shown. Left: spatial maps overlaid onto a 3D rendering of an MNI template brain. Right: ICA associated time courses (in black) and task profiles (in red, after convolution with the hemodynamic response); the correlation coefficient r_t was 0.77 and 0.78 for Networks 1 and 2, respectively. The color scale indicates t values.

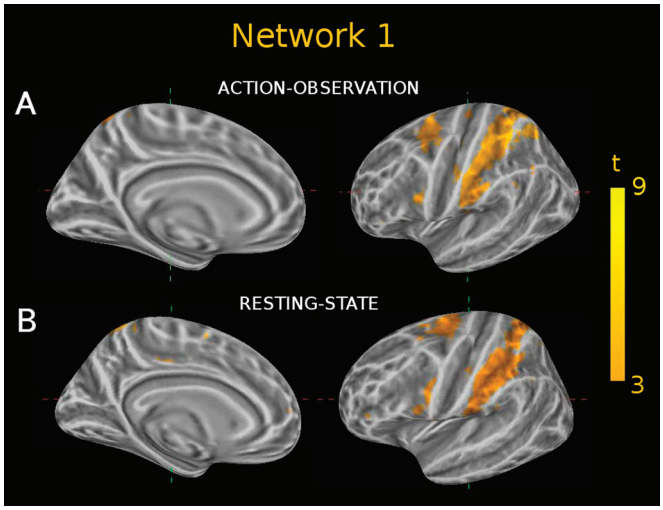

Figure 3. Network 1. ICA map related to action observation (*A*), in comparison with a spatially similar resting-state ICA map (*B*), shown on the lateral and medial aspects of the inflated brain (Freesurfer S/W package http://surfer.nmr.mgh.harvard.edu/). (*A*) ICA map MOVE run1-IC4; (*B*) ICA map REST-IC4. The percentage SO (relative to the task run) between the 2 maps was 52%.

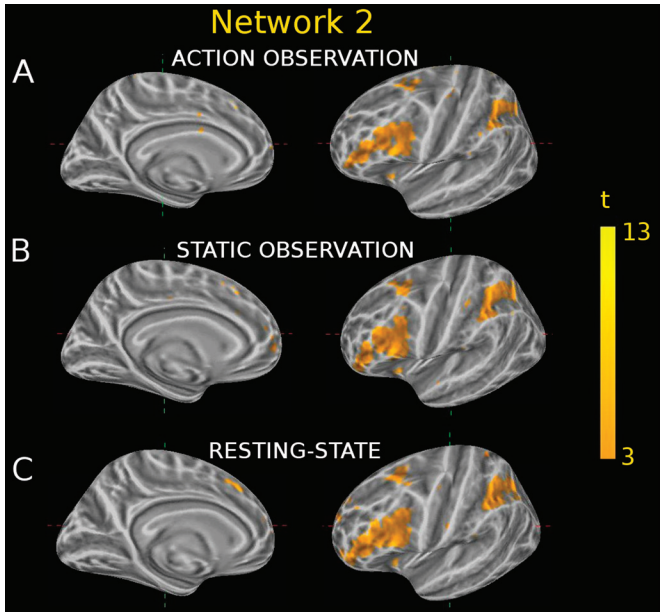

Figure 4. Network 2. ICA maps related to action (*A*) or to static (*B*) observation, in comparison with a spatially similar resting-state map (*C*), shown on the lateral and medial aspects of the inflated brain. (*A*) ICA map MOVE run2-IC2; (*B*) ICA map STAT run1-IC1; (*C*) ICA map REST-IC1. The percentage SO between map pairs *AB, BC,* and *AC* was 73%, 57%, and 63%, respectively.

Table 1
Spatial similarity between selected ICA maps

	Network 1 REST-IC4	Network 1 MOVE run2-IC3	Network 2 REST-IC1	Network 2 MOVE run1-IC5	Network 2 STAT run2-IC1
Network 1 MOVE run1-IC4	**0.567**	**0.685**	0.118	0.346	0.267
Network 2 MOVE run2-IC2	0.214	0.244	**0.623**	**0.679**	**0.849**
Network 2 STAT run1-IC1	0.237	0.319	**0.609**	**0.705**	**0.887**

Note: Values represent the correlation coefficient r_s between spatial components identified using ICA. Network 2 could be identified in both the action observation (MOVE) and the static-scene observation (STAT) runs. A high spatial similarity between maps is marked in bold font.

Table 2
Network 1: clusters specifically related to action observation

Region		ICA-MOVE runs					ICA-REST (IC4)				
		x	*y*	*z*	Size	*t*	*x*	*y*	*z*	Size	*t*
IPL	MOVE[a]	−42	−36	44	262		−42	−36	43	300	9.14
	run1-IC4	−38	−39	48	279	9.58					
	run2-IC3	−47	−33	41	246	8.67					
DLP cortex	MOVE[a]	−26	−7	55	55		−24	−6	57	81	6.06
	run1-IC4	−27	−6	54	57	10.03					
	run2-IC3	−25	−8	56	53	6.73					
Ventral premotor cortex	MOVE[a]	−48	6	28	38		−51	6	28	41	6.21
	run1-IC4	−49	6	30	27	6.89					
	run2-IC3	−47	6	25	48	5.88					

Note: *x*, *y*, *z* values are center-of-mass coordinates in the MNI space, expressed in mm. Cluster size is expressed in voxels. *t* values are relative to the activation peak.
[a]Mean values across runs.

Tables 2 and 3 report the center-of-mass coordinates of the main clusters of Networks 1 and 2, respectively. The centers of mass of clusters belonging to Network 1 were located more anteriorly in the parietal cortex, slightly more dorsally in the ventrolateral premotor region and more posteriorly in the dorsolateral premotor region, than those of Network 2 (see Fig. 2 and Tables 2 and 3).

The degree of SO between the 3 main clusters (parietal, dorsolateral premotor, and ventrolateral premotor) of the 2 networks related to action observation, and of the corresponding networks identified in the REST run, is shown in Table 4 (see also Fig. 5).

fMRI Data—Intersubject Variability

In each of the 14 subjects undergoing both the rest and the task runs, we found action observation spatial components having a corresponding component in their resting-state data. In 11 subjects, at least one of these components could be spatially associated to Network 1 identified in the group analysis, while for 7 of them, it could be associated to Network 2 (4 subjects had both). The mean (±SD) values across subjects of the r_s coefficient between the action observation–related and the corresponding resting-state maps found in the same subject were 0.466 ± 0.07 (range: 0.353–0.68) for Network 1 and 0.477 ± 0.09 (range: 0.33–0.62) for Network 2. Across-subjects values of the r_s coefficient between the individual and group action observation–related ICA maps were 0.29 ± 0.1 and 0.28 ± 0.09 for Network 1 and Network 2, respectively. Across-subjects values of the r_s coefficient between the individual and group resting-state ICA maps were 0.27 ± 0.1 and 0.31 ± 0.13 for Network 1 and Network 2, respectively. Finally, for the action observation data, the mean ± SD across subjects of r_t was 0.57 ± 0.09 and 0.49 ± 0.08 for Network 1 and Network 2, respectively.

Anatomical Connectivity

To test for repeatability, we computed the percent difference between the number of whole-brain fiber tracts, estimated via deterministic tractography from the 2 acquired DWI for each volunteer. The average (±SD) value across the 14 volunteers was 0.45 ± 0.36%.

Table 3
Network 2: clusters related to both action and static observation

Region		ICA observation runs					ICA-REST (IC1)				
		x	*y*	*z*	Size	*t*	*x*	*y*	*z*	Size	*t*
Posterior parietal cortex	STAT[a]	−40	−47	45	158		−38	−51	45	156	7.46
	run1-IC1	−40	−48	45	158	12.57					
	run2-IC1	−40	−46	45	159	10.74					
	MOVE[a]	−43	−44	43	127						
	run1-IC5	−47	−39	42	136	8.16					
	run2-IC2	−39	−48	44	118	8.03					
DLP cortex	STAT[a]	−28	5	54	28		−25	5	52	30	5.36
	run1-IC1	−28	5	55	15	5.06					
	run2-IC1	−27	5	52	41	12.66					
	MOVE[a]	−26	4	52	12						
	run1-IC5	−27	0	53	12	4.50					
	run2-IC2	−25	8	52	13	4.72					
Ventral premotor cortex/Broca area	STAT[a]	−44	21	20	219		−42	22	23	217	7.69
	run1-IC1	−44	21	19	215	8.57					
	run2-IC1	−43	21	20	223	9.11					
	MOVE[a]	−44	20	22	122						
	run1-IC5	−43	23	20	110	11.39					
	run2-IC2	−44	18	23	135	7.83					

Note: *x*, *y*, *z* values are center-of-mass coordinates in the MNI space, expressed in mm. Cluster size is expressed in voxels. *t* values are relative to the activation peak.
[a]Mean values across runs.

Table 4
Percent SO between resting-state and action observation ICA maps

Cluster	Network 1	Network 2
Posterior parietal	56.6	60.2
VLP	40.7	71.9
DLP	57.9	15.4

Note: Values represent percentage overlap between clusters belonging to the resting-state and action observation ICA maps, for the 2 parietofrontal networks identified in the group analysis. Percentage values are computed over the mean cluster volumes of the 2 corresponding action observation–related maps, identified in the 2 runs.

We next estimated the number of tracts connecting pairs of clusters of the REST-IC4 (the resting-state component associated with Network 1) and of the REST-IC1 (the resting-state component associated with Network 2) maps. The strongest connection was found between the posterior parietal (PPar) and the ventrolateral premotor (VLP) clusters (see Table 5). In REST-IC4, the fiber tracts connecting PPar and the dorsolateral premotor (DLP) cluster seem to originate specifically from the anterior and dorsal aspect of the PPar cluster (Fig. 6*A*). By contrast, the tracts connecting PPar and VLP appear to originate from the anterior and central portion of the PPar cluster and to reach the dorsal portion of the VLP cluster (Fig. 6*B*). Tracts were also identified between DLP and VLP (Fig. 6*C*).

The tracts connecting clusters of the REST-IC1 map are shown in Supplementary Fig. 3S.

Discussion

Three main conclusions can be derived from our findings. First, 2 parietofrontal networks active during the observation of hand actions, showing only partial overlap, can be reliably detected by ICA of fMRI data in healthy volunteers; one is more specifically related to the observation of reaching and grasping movements, the other is also active during the observation of a still hand and object. Second, 2 parietofrontal networks largely overlapping the observation-related ICA maps can be identified by ICA from resting-state fMRI data. Third, the coherent activity of these networks is at least in part supported by direct anatomical connections between their nodes.

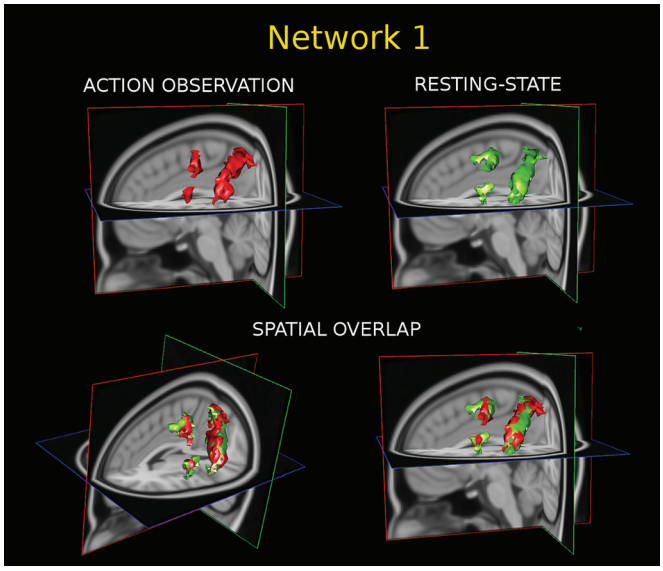

Figure 5. Illustration of spatial overlap between the 3 main clusters (parietal, dorsolateral premotor, and ventrolateral premotor) specifically related to action observation (Network 1), identified using task or rest conditions. Red: ICA, MOVE run1-IC4 component; green: ICA, REST-IC4 component. Top: 3D maps for the task condition (left) and for the rest condition (right). Bottom: Spatial overlap between clusters of the 2 maps, shown from 2 different angles to facilitate comparison.

Table 5
Anatomical connections between parietal and frontal clusters

Cluster pairs	Number of fiber tracts	
	Network 1 (REST-IC4)	Network 2 (REST-ICI)
PPar-VLP	323	160
PPar-DLP	251	—
DLP-VLP	89	34.5

Note: Median values across 16 subjects of the number of fiber tracts connecting the posterior parietal (PPar) clusters with premotor clusters (DLP and VLP) for the 2 resting-state components of interest (REST-IC4 and REST-IC1). DLP-VLP connections are also shown. The data do not include areas of overlap between DLP and VLP clusters of the 2 resting-state components.

Observation-Related Parietofrontal Networks

In the monkey, observation of an acting hand induces activity in rostral area F5 and area 45B (Nelissen et al. 2005), which are thought to correspond to human Brodmann areas (BAs) 44 and 45, respectively (Petrides and Pandya 2002). In humans, PET and fMRI studies have consistently shown that the observation of an individual acting upon an object activates a parietofrontal system, including intraparietal sulcus (IPS) and inferior parietal lobule (IPL), VLP, the caudal part of the inferior frontal gyrus (IFG), and sometimes DLP (Rizzolatti and Craighero 2004; Caspers et al. 2010). The coordinates of action observation–related clusters, identified in the present study using either GLM (see Supplementary Material) or ICA (Network 1), are consistent with those found in a recent meta-analysis (Caspers et al. 2010); for instance, they are less than 5 mm apart, in any direction, from the peak coordinates reported for the "Observation right hand" category (Caspers et al. 2010).

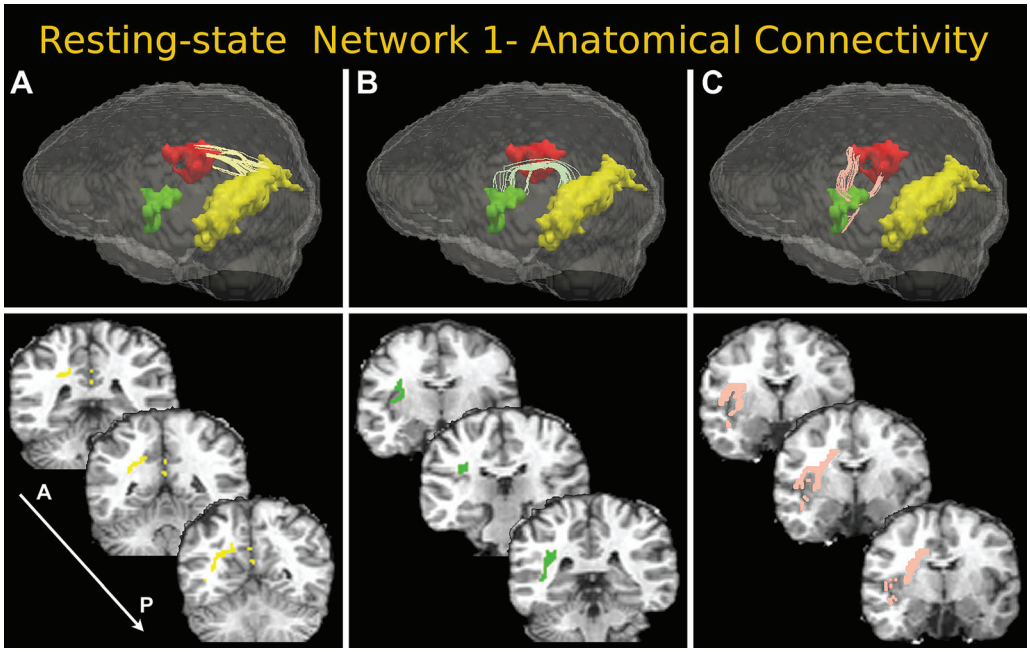

Figure 6. Fiber bundles connecting pairs of clusters of the REST-IC4 component, as assessed by DWI, PAS, and deterministic tractography. For a clearer visualization, the fibers shown were tracked only within an exclusion mask, which was obtained as follows: first, a map, where each voxel value was set to the number of streamlines intersecting it, was computed; then, a sum of this map values over a 3-voxel cubic neighborhood was computed for each voxel; finally, the latter map was thresholded at a value of 15, and the fibers were then tracked. Top: 3D visualization of ICA clusters and connecting fiber bundles; cluster colors: yellow: PPar; red: DLP; green: VLP. Abbreviations as in Table 4. Bottom: Coronal sections showing the location of connecting tracts in the white matter of the left hemisphere. Subfigures A,B,C illustrate connections between different cluster pairs (see main text).

Notably, ICA revealed 2 parietofrontal maps, with likely different functional properties. The first network, which could be reliably identified only from the action observation runs, is likely involved in coding dynamic hand actions; the second network, which could be identified from both the action observation and the static-scene observation runs, is probably related to a more general representation of hand-and-object complexes (not necessarily dynamic). In this respect, our findings extend those of a recent fMRI work, differentiating object-related and action observation–related activity in the human brain (Tremblay and Small 2011). Object-directed actions are strictly linked to the visual coding of objects and their affordances, which are represented near and inside IPS (Grafton and Hamilton 2007) as well as in DLP (Grafton et al. 1997). Indeed, 3D features of objects are encoded by neurons in the caudal IPS and in the anterior intraparietal area and are likely to be used for the guidance of hand manipulation (Gallese et al. 1994; Murata et al. 1996; Nakamura et al. 2001). The parietal cortex and VLP are anatomically connected (Matelli and Luppino 2001; Rozzi et al. 2006; Borra et al. 2008), forming parallel circuits involved in the transformation of intrinsic properties of objects (size and shape) into the appropriate motor acts to interact with them (Rizzolatti and Luppino 2001). In the monkey brain, ventral premotor area F5 contains different motor-related neurons; for instance, "mirror" neurons active during both action observation and action execution and "canonical" neurons responding to the execution of actions and to the sight of objects that afford these actions but not to action observation per se (Rizzolatti et al. 1988; Gallese et al. 1996). Our findings concerning the premotor cortex (but not the parietal cortex) differ from those of Tremblay and Small (2011) who suggested that, within the human premotor cortex, neurons with canonical properties are mainly located in dorsal VLP, whereas action observation–related neurons mainly in ventral VLP. Further studies involving also actual movement execution are needed in order to assess the spatial distribution of areas with mirror neurons properties within the identified networks.

Only few studies have described patterns of fMRI functional connectivity in parietofrontal circuits related to action or object observation, and, to our knowledge, none using ICA. Using psychophysiological interaction analysis in a task where subjects were asked to judge object graspability, Hattori et al. (2009) provided evidence for 2 different networks involving the left IPL and VLP; one was active only during judgment of graspable objects, the other during judgment of either graspable or nongraspable objects. Other functional connectivity studies dealt with the observation of complex intransitive actions, such as speech-associated gestures (Skipper et al. 2007) and symbolic gestures and pantomimes (Xu et al. 2009; Emmorey et al. 2010), or focused on networks involved in the inhibition of automatic imitation (Bien et al. 2009) and are therefore not directly comparable with our findings.

Functional Resting-State and Anatomical Connectivity of Parietofrontal Circuits

RSFC approaches have been increasingly applied to characterize functional networks (Smith et al. 2009; Koyama et al. 2010) and to parcellate regions (Kim et al. 2010; Kelly et al. 2010; Craddock et al. 2011) in the human brain. For instance, by examining correlations between spontaneous BOLD fluctuations in a seed region of interest and in each other brain voxel, Vincent and colleagues (Vincent et al. 2008) described different parietofrontal networks involving the superior parietal lobule, anterior inferior, and posterior IPL. A direct

comparison of resting-state and task-related activity in the same subjects, using data-driven approaches, can rarely been found in the literature (see Moeller et al. 2009); however, there is recent evidence that interindividual differences in task-induced activity are predicted by resting-state properties (Mennes et al. 2010, 2011). Moreover, few studies have directly compared RSFC with structural connectivity (Hagmann et al. 2008; Damoiseaux and Greicius 2009; Ystad et al. 2011).

The 2 parietofrontal networks identified in the present study bears similarities to RSFC networks described in earlier papers—for example, van de Ven et al. (2004) for Network 1 and van de Ven et al. (2004), Fox et al. (2005), Damoiseaux et al. (2006), and van den Heuvel et al. (2008) for Network 2.

We are not aware of published electrophysiological studies in primates based on simultaneous recordings from the parietal and frontal cortices, which would provide direct experimental evidence for the neural basis of the RSFC networks identified here. Nevertheless, the close spatial correspondence between the 2 parietofrontal circuits identified at rest and those found during action observation, as well as the existence of anatomical pathways between their parietal and frontal nodes, strongly support this hypothesis. Other indirect evidence for resting-state coherent neural networks involving posterior parietal and frontal premotor neural populations come from anatomical connectivity data in monkeys (Matelli and Luppino 2001; Petrides and Pandya 2009) and, more recently, in humans (e.g., Croxson et al. 2005; Anwander et al. 2007; Tomassini et al. 2007; Frey et al. 2008).

Available data suggest that the strength of RSFC correlates positively with structural connectivity strength (Skudlarski et al. 2008), even if BOLD signal correlations can also be mediated by indirect (polysynaptic) connections. In a recent fMRI study, Kelly et al. (2010) showed that the ventrolateral frontal areas of the human brain exhibit patterns of RSFC consistent with patterns of anatomical connectivity observed in the macaque. Specifically, BA 44 located in the IFG pars opercularis exhibited positive correlations with IFG pars triangularis (BA 45), VLP (BA 6), BA 8, and the rostral DLP. In the parietal cortex, correlations were primarily restricted to the ventral part of the posterior supramarginal gyrus and the adjacent angular gyrus. BA 45 exhibited a similar pattern of correlations, but relative to BA 44, greater positive correlations were found with the angular gyrus. This pattern resembles in part the findings of the present study.

The existence of direct anatomical connections among the nodes of the identified functional networks was tested here using a new approach which combines HARDI—able to better resolve complex intravoxel structures in comparison to diffusion tensor imaging—with the new reduced encoding PAS-MRI technique.

The location of estimated tracts is consistent with different subdivisions (mainly the second and the third one) of the superior longitudinal fascicle, the major association fiber pathway connecting posterior parietal and frontal regions (Makris et al. 2005). Our data thus provide additional direct evidence that the nodes of human resting-state parietofrontal circuits are anatomically linked.

Limitations of the Study

In order to increase the sampling of the hemodynamic response and minimize the influence of respiration-induced aliased confounds in the BOLD signal, we chose to acquire fMRI data at a relatively high temporal resolution. As a consequence, we could sample BOLD activity from one hemisphere only; moreover, functional images covered the parietal and frontal cortices but not other cortical regions, such as the anterior part of the temporal lobe. Therefore, we were not able to investigate the similarities and differences between the parietofrontal networks of the 2 hemispheres nor the interhemispheric connectivity of homologous regions or frontotemporal circuits.

Notably, since the main goal of the present study was to compare parietofrontal networks during rest and observation tasks, we used a data-driven approach to identify the main nodes of these networks. Further investigations may examine the nature of effective connectivity within these circuits, using approaches, such as structural equation modeling (McIntosh and Gonzalez-Lima 1994) and dynamic causal modeling (Friston et al. 2003; Grol et al. 2007).

Concluding Remarks

Our findings that 2 parietofrontal networks identified at rest show a substantial spatial similarity to those involved in action observation lend further support to the hypothesis of an ongoing coherent activity within functionally linked cortical circuits in the human brain. It will be interesting to explore whether, and to which extent, such coherence is preserved in patients for which an impairment of the action observation/mirror system has been hypothesized (Iacoboni and Mazziotta 2007; Rizzolatti and Fabbri-Destro 2008), such as in autistic spectrum disorders.

Supplementary Material

Supplementary material can be found at: http://www.cercor.oxfordjournals.org/

Funding

Supported by grants of Istituto Italiano di Tecnologia, BMI Project 2009-2011 and of Regione Emilia Romagna, Programma di Ricerca Regione-Università 2007-2009, to C.A.P. The support of the Fondazione Cassa di Risparmio di Modena to the Modena MR center is gratefully acknowledged.

Conflict of Interest: None declared.

References

Abou-Elseoud A, Starck T, Remes J, Nikkinen J, Tervonen O, Kiviniemi V. 2010. The effect of model order selection in group PICA. Hum Brain Mapp. 31:1207–1216.

Anwander A, Tittgemeyer M, von Cramon DY, Friederici AD, Knosche TR. 2007. Connectivity-based parcellation of Broca's area. Cereb Cortex. 17:816–825.

Ashburner J, Friston KJ. 2005. Unified segmentation. Neuroimage. 26:839–851.

Beckmann CF, Smith SM. 2004. Probabilistic independent component analysis for functional magnetic resonance imaging. IEEE Trans Med Imaging. 23:137–152.

Bien N, Roebroeck A, Goebel R, Sack AT. 2009. The brain's intention to imitate: the neurobiology of intentional versus automatic imitation. Cereb Cortex. 19:2338–2351.

Borra E, Belmalih A, Calzavara R, Gerbella M, Murata A, Rozzi S, Luppino G. 2008. Cortical connections of the macaque anterior intraparietal (AIP) area. Cereb Cortex. 18:1094–1111.

Calhoun VD, Adali T, Pearlson GD, Pekar JJ. 2001. A method for making group inferences from functional MRI data using independent component analysis. Hum Brain Mapp. 14:140–151.
Caspers S, Zilles K, Laird AR, Eickhoff SB. 2010. ALE meta-analysis of action observation and imitation in the human brain. Neuroimage. 50:1148–1167.
Catmur C, Walsh V, Heyes C. 2009. Associative sequence learning: the role of experience in the development of imitation and the mirror system. Philos Trans R Soc Lond B Biol Sci. 364: 2369–2380.
Cook PA, Bai Y, Nedjati-Gilani S, Seunarine KK, Hall MG, Parker GJ, Alexander DC. 2006. Camino: open-source diffusion-MRI reconstruction and processing. Proceedings of the 14th Annual Meeting of ISMRM; 2006 May 6–12; Seattle (WA). p. 2759.
Cox RW. 1996. AFNI: software for analysis and visualization of functional magnetic resonance neuroimages. Comput Biomed Res. 29:162–173.
Craddock RC, James GA, Holtzheimer PE III, Hu XP, Mayberg HS. 2011. A whole brain fMRI atlas generated via spatially constrained spectral clustering. Hum Brain Mapp. doi: 10.1002/hbm.21333.
Croxson PL, Johansen-Berg H, Behrens TE, Robson MD, Pinsk MA, Gross CG, Richter W, Richter MC, Kastner S, Rushworth MF. 2005. Quantitative investigation of connections of the prefrontal cortex in the human and macaque using probabilistic diffusion tractography. J Neurosci. 25:8854–8866.
Damoiseaux JS, Greicius MD. 2009. Greater than the sum of its parts: a review of studies combining structural connectivity and resting-state functional connectivity. Brain Struct Funct. 213: 525–533.
Damoiseaux JS, Rombouts SA, Barkhof F, Scheltens P, Stam CJ, Smith SM, Beckmann CF. 2006. Consistent resting-state networks across healthy subjects. Proc Natl Acad Sci U S A. 103:13848–13853.
Deco G, Jirsa VK, McIntosh AR. 2011. Emerging concepts for the dynamical organization of resting-state activity in the brain. Nat Rev Neurosci. 12:43–56.
Doucet G, Naveau M, Petit L, Delcroix N, Zago L, Crivello F, Jobard G, Tzourio-Mazoyer N, Mazoyer B, Mellet E, et al. 2011. Brain activity at rest: a multiscale hierarchical functional organization. J Neurophysiol. 105:2753–2763.
Emmorey K, Xu J, Gannon P, Goldin-Meadow S, Braun A. 2010. CNS activation and regional connectivity during pantomime observation: no engagement of the mirror neuron system for deaf signers. Neuroimage. 49:994–1005.
Forman SD, Cohen JD, Fitzgerald M, Eddy WF, Mintun MA, Noll DC. 1995. Improved assessment of significant activation in functional magnetic resonance imaging (fMRI): use of a cluster-size threshold. Magn Reson Med. 33:636–647.
Fox MD, Snyder AZ, Vincent JL, Corbetta M, Van E, Raichle ME. 2005. The human brain is intrinsically organized into dynamic, anticorrelated functional networks. Proc Natl Acad Sci U S A. 102:9673–9678.
Frey S, Campbell JS, Pike GB, Petrides M. 2008. Dissociating the human language pathways with high angular resolution diffusion fiber tractography. J Neurosci. 28:11435–11444.
Friston KJ, Ashburner JT, Kiebel S, Nichols TE, Penny WD. 2006. Statistical parametric mapping: the analysis of functional brain images. London: Elsevier.
Friston KJ, Harrison L, Penny W. 2003. Dynamic causal modelling. Neuroimage. 19:1273–1302.
Friston KJ, Holmes A, Worsley K, Poline JB, Frith C, Frackowiak R. 1995. Statistical parametric maps in functional imaging: a general linear approach. Hum Brain Mapp. 2:189–210.
Gallese V. 2009. Motor abstraction: a neuroscientific account of how action goals and intentions are mapped and understood. Psychol Res. 73:486–498.
Gallese V, Fadiga L, Fogassi L, Rizzolatti G. 1996. Action recognition in the premotor cortex. Brain. 119:593–609.
Gallese V, Murata A, Kaseda M, Niki N, Sakata H. 1994. Deficit of hand preshaping after muscimol injection in monkey parietal cortex. Neuroreport. 5:1525–1529.
Grafton ST, Fadiga L, Arbib MA, Rizzolatti G. 1997. Premotor cortex activation during observation and naming of familiar tools. Neuroimage. 6:231–236.
Grafton ST, Hamilton AF. 2007. Evidence for a distributed hierarchy of action representation in the brain. Hum Mov Sci. 26:590–616.
Grol MJ, Majdandzic J, Stephan KE, Verhagen L, Dijkerman HC, Bekkering H, Verstraten FA, Toni I. 2007. Parieto-frontal connectivity during visually guided grasping. J Neurosci. 27:11877–11887.
Hagmann P, Cammoun L, Gigandet X, Meuli R, Honey CJ, Wedeen VJ, Sporns O. 2008. Mapping the structural core of human cerebral cortex. PLoS Biol. 6:e159.
Hattori N, Shibasaki H, Wheaton L, Wu T, Matsuhashi M, Hallett M. 2009. Discrete parieto-frontal functional connectivity related to grasping. J Neurophysiol. 101:1267–1282.
Iacoboni M, Mazziotta JC. 2007. Mirror neuron system: basic findings and clinical applications. Ann Neurol. 62:213–218.
Ioannides AA. 2007. Dynamic functional connectivity. Curr Opin Neurobiol. 17:161–170.
Jansons KM, Alexander DC. 2003. Persistent angular structure: new insights from diffusion magnetic resonance imaging data. Inverse Probl. 19:1031–1046.
Jiang Q, Alexander DC, Ding GL, Zhang ZG, Pourabdollah Nejad DS, Zhang L, Li L, Hu J, Bagherebadian H, Chopp M. 2007. White matter reorganization after stroke measured by Gaussian DTI, q-ball, and PAS MRI. Proceedings of the Joint Annual Meeting ISMRM-ESMRMB; 2007 May 19–25; Berlin (Germany). p. 66.
Kelly C, Uddin LQ, Shehzad Z, Margulies DS, Castellanos FX, Milham MP, Petrides M. 2010. Broca's region: linking human brain functional connectivity data and non-human primate tracing anatomy studies. Eur J Neurosci. 32:383–398.
Kim JH, Lee JM, Jo HJ, Kim SH, Lee JH, Kim ST, Seo SW, Cox RW, Na DL, Kim SI, et al. 2010. Defining functional SMA and pre-SMA subregions in human MFC using resting state fMRI: functional connectivity-based parcellation method. Neuroimage. 49: 2375–2386.
Koyama MS, Kelly C, Shehzad Z, Penesetti D, Castellanos FX, Milham MP. 2010. Reading networks at rest. Cereb Cortex. 20:2549–2559.
Makris N, Kennedy DN, McInerney S, Sorensen AG, Wang R, Caviness VS Jr, Pandya DN. 2005. Segmentation of subcomponents within the superior longitudinal fascicle in humans: a quantitative, in vivo, DT-MRI study. Cereb Cortex. 15:854–869.
Matelli M, Luppino G. 2001. Parietofrontal circuits for action and space perception in the macaque monkey. Neuroimage. 14:S27–S32.
McIntosh AR, Gonzalez-Lima F. 1994. Structural equation modeling and its application to network analysis in functional brain imaging. Hum Brain Mapp. 2:2–22.
Mennes M, Kelly C, Zuo XN, Di MA, Biswal BB, Castellanos FX, Milham MP. 2010. Inter-individual differences in resting-state functional connectivity predict task-induced BOLD activity. Neuroimage. 50:1690–1701.
Mennes M, Zuo XN, Kelly C, Di MA, Zang YF, Biswal B, Castellanos FX, Milham MP. 2011. Linking inter-individual differences in neural activation and behavior to intrinsic brain dynamics. Neuroimage. 54:2950–2959.
Moeller S, Nallasamy N, Tsao DY, Freiwald WA. 2009. Functional connectivity of the macaque brain across stimulus and arousal states. J Neurosci. 29:5897–5909.
Murata A, Gallese V, Kaseda M, Sakata H. 1996. Parietal neurons related to memory-guided hand manipulation. J Neurophysiol. 75: 2180–2186.
Nakamura H, Kuroda T, Wakita M, Kusunoki M, Kato A, Mikami A, Sakata H, Itoh K. 2001. From three-dimensional space vision to prehensile hand movements: the lateral intraparietal area links the area V3A and the anterior intraparietal area in macaques. J Neurosci. 21:8174–8187.
Nelissen K, Luppino G, Vanduffel W, Rizzolatti G, Orban GA. 2005. Observing others: multiple action representation in the frontal lobe. Science. 310:332–336.
Oldfield RC. 1971. The assessment and analysis of handedness: the Edinburgh inventory. Neuropsychologia. 9:97–113.

Ortigue S, Sinigaglia C, Rizzolatti G, Grafton ST. 2010. Understanding actions of others: the electrodynamics of the left and right hemispheres. A high-density EEG neuroimaging study. PLoS One. 5:e12160.
Pagnoni G, Cekic M, Drake DF, Fornwalt F, Raison CL, Berns GS. 2006. Topography and dynamics of resting state networks during meditation. Soc. Neurosci. Abstr. 364.12/FF19; 2006 (http://www.sfn.org/).
Petrides M, Pandya DN. 2002. Comparative cytoarchitectonic analysis of the human and the macaque ventrolateral prefrontal cortex and corticocortical connection patterns in the monkey. Eur J Neurosci. 16:291–310.
Petrides M, Pandya DN. 2009. Distinct parietal and temporal pathways to the homologues of Broca's area in the monkey. PLoS Biol. 7:e1000170.
Rizzolatti G, Camarda R, Fogassi L, Gentilucci M, Luppino G, Matelli M. 1988. Functional organization of inferior area 6 in the macaque monkey. II. Area F5 and the control of distal movements. Exp Brain Res. 71:491–507.
Rizzolatti G, Craighero L. 2004. The mirror-neuron system. Annu Rev Neurosci. 27:169–192.
Rizzolatti G, Fabbri-Destro M. 2008. The mirror system and its role in social cognition. Curr Opin Neurobiol. 18:179–184.
Rizzolatti G, Luppino G. 2001. The cortical motor system. Neuron. 31:889–901.
Rozzi S, Calzavara R, Belmalih A, Borra E, Gregoriou GG, Matelli M, Luppino G. 2006. Cortical connections of the inferior parietal cortical convexity of the macaque monkey. Cereb Cortex. 16:1389–1417.
Sadaghiani S, Hesselmann G, Friston KJ, Kleinschmidt A. 2010. The relation of ongoing brain activity, evoked neural responses, and cognition. Front Syst Neurosci. 4:20.
Skipper JI, Goldin-Meadow S, Nusbaum HC, Small SL. 2007. Speech-associated gestures, Broca's area, and the human mirror system. Brain Lang. 101:260–277.
Skudlarski P, Jagannathan K, Calhoun VD, Hampson M, Skudlarska BA, Pearlson G. 2008. Measuring brain connectivity: diffusion tensor imaging validates resting state temporal correlations. Neuroimage. 43:554–561.
Smith SM. 2002. Fast robust automated brain extraction. Hum Brain Mapp. 17:143–155.
Smith SM, Fox PT, Miller KL, Glahn DC, Fox PM, Mackay CE, Filippini N, Watkins KE, Toro R, Laird AR, et al. 2009. Correspondence of the brain's functional architecture during activation and rest. Proc Natl Acad Sci U S A. 106:13040–13045.
Smith SM, Jenkinson M, Woolrich MW, Beckmann CF, Behrens TE, Johansen-Berg H, Bannister PR, De LM, Drobnjak I, Flitney DE, et al. 2004. Advances in functional and structural MR image analysis and implementation as FSL. Neuroimage. 23(Suppl 1):S208–S219.
Sweet A, Alexander DC. 2010. Reduced encoding persistent angular structure. Proceedings of the 18th Annual Meeting of ISMRM; 2010 May 1–7; Stockholm (Sweden). p. 572.
Tomassini V, Jbabdi S, Klein JC, Behrens TE, Pozzilli C, Matthews PM, Rushworth MF, Johansen-Berg H. 2007. Diffusion-weighted imaging tractography-based parcellation of the human lateral premotor cortex identifies dorsal and ventral subregions with anatomical and functional specializations. J Neurosci. 27:10259–10269.
Tononi G. 2010. Information integration: its relevance to brain function and consciousness. Arch Ital Biol. 148:299–322.
Tremblay P, Small SL. 2011. From language comprehension to action understanding and back again. Cereb Cortex. 21:1166–1177.
Tuch DS, Weisskoff RM, Belliveau JW, Wedeen VJ. 1999. High angular resolution diffusion imaging of the human brain. Proceedings of the 7th Annual Meeting of ISMRM; 1999 May 22–28; Philadelphia (PA). p. 321.
van de Ven V, Formisano E, Prvulovic D, Roeder CH, Linden DE. 2004. Functional connectivity as revealed by spatial independent component analysis of fMRI measurements during rest. Hum Brain Mapp. 22:165–178.
van den Heuvel M, Mandl R, Hulshoff PH. 2008. Normalized cut group clustering of resting-state FMRI data. PLoS One. 3:e2001.
Vincent JL, Kahn I, Snyder AZ, Raichle ME, Buckner RL. 2008. Evidence for a frontoparietal control system revealed by intrinsic functional connectivity. J Neurophysiol. 100:3328–3342.
Xu J, Gannon PJ, Emmorey K, Smith JF, Braun AR. 2009. Symbolic gestures and spoken language are processed by a common neural system. Proc Natl Acad Sci U S A. 106:20664–20669.
Ystad M, Hodneland E, Adolfsdottir S, Haasz J, Lundervold AJ, Eichele T, Lundervold A. 2011. Cortico-striatal connectivity and cognition in normal aging: a combined DTI and resting state fMRI study. Neuroimage. 55:24–31.
Yushkevich PA, Piven J, Hazlett HC, Smith RG, Ho S, Gee JC, Gerig G. 2006. User-guided 3D active contour segmentation of anatomical structures: significantly improved efficiency and reliability. Neuroimage. 31:1116–1128.
Zuo XN, Kelly C, Adelstein JS, Klein DF, Castellanos FX, Milham MP. 2010. Reliable intrinsic connectivity networks: test-retest evaluation using ICA and dual regression approach. Neuroimage. 49:2163–2177.